Proceedings of the 21st ICSMGE, Vienna, Austria, 14 – 19 June 2026. Pistrol, Adam & Schweiger (eds.)
Published by: ÖGG, Austrian Society for Geomechanics, Salzburg, Austria, ISBN 978-3-9503898-4-5
https://doi.org/10.53243/ICSMGE2026-1190

A novel grouped caisson–plate system for offshore anchoring: Finite element analyses

Lau Fogh, Andrea Franza, Luis Felipe Prada-Sarmiento, Lars Vabbersgaard Andersen
Department of Civil and Architectural Engineering, Aarhus Universitet, Denmark, lfo@cae.au.dk

ABSTRACT: This paper introduces a novel grouped anchoring concept for floating offshore wind turbines (FOWTs), aimed at enhancing the efficiency and robustness of mooring systems. The proposed system, termed the *caisson–embedded-plate-anchor system* (CEPAS), consists of a suction caisson connected to one or more embedded plate anchors via intermediate chains. The concept builds on the hypothesis that a configuration of interconnected, smaller anchoring elements can outperform a single large anchor of equivalent material volume by mobilising soil resistance more effectively. To investigate this, finite element analyses are conducted to study the load–displacement behaviour and ultimate capacity of various CEPAS configurations. The results reveal that the system's performance depends strongly on the relative geometry and, thus, the geotechnical interaction between its components, with certain configurations exhibiting increased stiffness and load capacity. Comparative analyses with single caissons suggest that the CEPAS is a promising offshore anchoring solution, with mechanical and adaptability advantages over conventional single-element designs.

KEYWORDS: floating offshore wind turbines, grouped anchors, suction caisson, plate anchor.

1 INTRODUCTION

The world urgently needs renewable sources of energy to tackle climate change and the depletion of fossil fuel reserves. Concurrently, global electricity demand is rising significantly. This context motivates the use of offshore renewable energy technologies. Although bottom-fixed offshore wind turbines are cost-competitive with fossil fuels, they are only feasible near-shore in many regions, such as North America, Oceania and parts of Southeast Asia (Barter et al., 2020). Furthermore, near-shore areas may also face limitations due to spatial constraints and aesthetic concerns. As a result, the development of floating offshore wind turbine (FOWT) technologies has accelerated in the last decade (International Energy Agency, 2019). Currently, FOWTs have high capital expenditures, with mooring lines and anchors contributing significantly to costs. To date, expertise in anchoring has been transferred from the oil and gas sector to the FOWT sector (Stehly et al., 2020); however, differing reliability demands between these two offshore applications creates an opportunity to further optimise anchoring systems for FOWTs based on plates and caissons, the latter two collectively referred to as *anchors* in this paper.

Several studies have confirmed the need for innovation in offshore foundation engineering, relying on reduced-scale experiments for hypothesis testing. Among others, Walker and Taylor (1984) tested drag anchors connected in tandem for the restraint of ships; their experiments indicated an increase in the load capacity of tandem drag anchors compared with the sum of individual elements. However, this came at the cost of specific manufacturing requirements of welding the fluke open to prevent the load from the aft anchor closing the fluke of the forward anchor. In general, care must be taken during manufacturing and installation to ensure the intended behaviour of foundation systems working in tandem. Dührkop et al. (2010) tested winged piles, which are piles fitted with locally tied plates at mid-depth. They observed increased lateral capacity compared with regular piles, suggesting that closely spaced piles and plates can improve the strength-to-weight ratio. Similarly, as a modified single foundation concept, Rui et al. (2024) proposed the *caisson–plate gravity anchor*, which consists of a suction caisson beneath a surface gravity plate, tied together to form a single anchor. The caisson–plate gravity anchor tackles the shortcomings of using an isolated suction caisson in a shared anchor configuration: i) too low vertical uplift resistance, ii) trench formation in front of the caisson. The plate's action, combined with its self-weight, increased uplift capacity and improved installation. Additionally, Rui et al. (2024) argued that attaching the mooring lines directly to the surface plate, rather than along the suction caisson, can reduce the risk of trench formation along the embedded section of the mooring line. This highlights the dependency of trenching and soil disturbance on the configuration and condition of the embedded line. These studies provide valuable insights for the development of innovative anchoring concepts.

To address the improvement of FOWT positional restraining systems, we propose a novel concept of *grouped anchors*, composed of plates and caissons interconnected by intermediate chains and functioning as a system of different anchor types working in tandem. The central hypothesis is that relatively closely spaced, interconnected, smaller anchors can outperform a single, larger foundation of equal material volume. This is expected to apply depending on whether the grouped anchors act as a composed foundation system (jointly mobilising a given soil volume) or as serial elements (mobilising soil resistance in distinct, non-overlapping volumes). Theoretically, grouped anchors have the potential to achieve high strength-to-weight and stiffness-to-weight ratios, as observed in onshore foundation and retaining systems (Cerfontaine, et al., 2023). For instance, pile groups and piled rafts connected by rigid or flexible surface elements, twin retaining walls, and soil nailing behind retaining structures illustrate how distributed but interconnected, relatively small foundations can deliver improved serviceability and capacity performance for the same amount of material, by mobilising the resistance of a greater soil volume. However, the design and construction of such foundations or retaining systems is inevitably more complex than for single elements.

This paper presents the proposed grouped anchor concept and, in the case of a single external mooring line, provides finite element results regarding the load–displacement response and for quantifying the load capacity of the grouped anchors under inclined monotonic loads. To quantify the efficiency of grouped anchors, their performance is compared against reference isolated caissons and single plates to obtain percentage variations in small deformation stiffness and load capacity at the nominal displacement level.

2 PRESENTATION OF GROUPED ANCHOR CONCEPT

The proposed grouped anchor consists of a single suction caisson connected to either one or multiple mooring lines, each linked via an embedded plate and an intermediate chain. This novel system is referred to as the *caisson–embedded-plate-anchor system* (CEPAS).

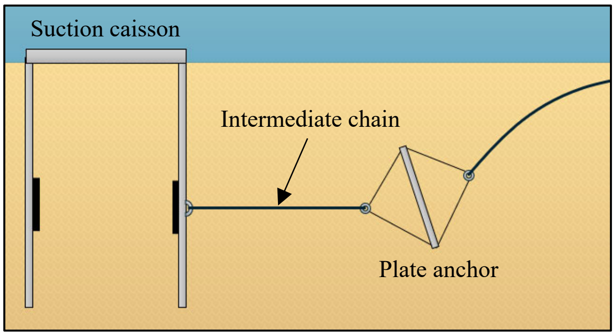

Figure 1. Schematic of a novel grouped anchor concept with single plate anchor.

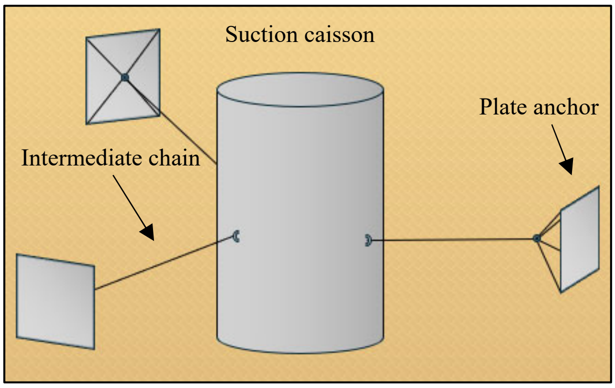

Figure 2. Schematic of novel grouped anchor with multiple plates.

Figure 1 illustrates a schematic of the grouped anchor for a single external mooring line, showing how the plate anchor is connected to the external mooring line and the intermediate chain by a shank, along with the caisson's internal reinforcement at the padeye. Figure 2 shows a schematic of how a CEPAS could be involved in a shared anchor setup for FOWTs.

As starting hypotheses of this research, a CEPAS may have several advantages over a single caisson, namely: (a) grouped anchors distribute steel over two components, increasing the total stiffness- and strength-to-weight ratios of the anchor; (b) the embedded plate can prevent trench formation in front of the caisson as it constrains the intermediate chain in its vicinity; (c) the embedded plate can sustain the vertical component of the external load transmitted by the external mooring line thus resulting in a mostly horizontal load on the caisson; furthermore, (d) the flexibility and possible slack of the intermediate mooring line can be controlled to improve the load-transfer between the plate and the caisson (e.g. the plate alone can resist loads in the serviceability range, thus limiting cyclic loading on the caisson). This paper addresses hypothesis (a) by studying the load-transfer mechanism of the CEPAS with nonlinear finite element analyses (FEA). Furthermore, the resistance and stiffness of CEPAS is compared to (i) the caisson and plate as components alone and (ii) a caisson with an extension of the skirt length to equal the steel volume of the group. The load capacities will be evaluated with finite element limit analysis (FELA) as the computational expense is lower, while the stiffnesses will be evaluated with FEA. The paper describes the efficiency of the grouped system through selected normalisations of these stiffnesses and load capacities. The hypotheses (b)–(d) are not addressed in this paper, but their confirmation will be targeted by future research.

3 CASE STUDY AND METHODOLOGY

The geometries of the case studies and the simplifications of the boundary conditions are chosen to yield practically relevant results. Figure 3 shows a schematic diagram of the considered grouped anchor in a uniform sand profile under a monotonic load imposed at the embedded plate. The height and diameter of the caisson are $H_c = 5.0$ m and $D_c = 4.0$ m, respectively. The plate anchor is square with a side length L_p of either 1.0 m or 2.0 m, to study the influence of the size of the plate relative to the caisson while keeping the length of the horizontal intermediate chain fixed at $L_\mathrm{i} = 6.0$ m and the depth of the padeye on the caisson fixed at $z_p = 3.5$ m. The thickness of the plate is $T_p = L_p/10$, and the thickness of the caisson skirt is $T_c = R_c/50$, while the thickness of the top of the caisson is set to $2T_c$. For simplicity, embedded plate anchors are purely vertical and subjected to an external load vector $\mathbf{F} = [H, V]^T$ with an inclination θ to the horizontal (omitting both the eccentricity in the load resulting from the shank as well as the modelling of the embedded part of the external mooring line). When the magnitude of $\mathbf{F}$ is equal to either of the components of the vector, that component is simply written. Load-transfer mechanisms are computed under purely horizontal loads (i.e. $\theta = 0°$, $\mathbf{F} = [H, 0]^T$), while, on the other hand, displacement-based load capacities are computed under inclined loading ($0° \leq \theta \leq 90°$, $\mathbf{F} = [H, V]^T$).

As materials, for the frictional granular soil, the Mohr–Coulomb (MC) constitutive model is selected with the friction angle $\varphi = 37.0°$, an associated flow rule (to have comparable FEA and FELA results), Young's modulus $E_s = 20.0$ MPa, Poisson's ratio $\nu_s = 0.25$, coefficient of lateral earth pressure at rest $K_0 = 1 - \sin\varphi$, and a submerged unit-weight of $9.5\ \mathrm{kN/m^3}$. Steel is described as a linear elastic and isotropic material with $E = 210$ GPa, $\nu = 0.30$, which is adopted for the caisson skirt, caisson top and plate anchor. To emulate a perfectly wished-in-place installation, the submerged unit weight of steel is also set initially to $9.5\ \mathrm{kN/m^3}$. Figure 4 shows the soil domain and mesh used in the FEA, while the FELA simulations use a similar domain. The analysis steps include: (1) model initialisation with wished-in-place structures and all boundaries, except for the ground surface (i.e. the mudline) fixed in the normal direction, (2) geo-static initial stress application, (3) monotonic load application.

Two commercial programs are employed for the FEA analyses to enable a numerical cross-verification: Abaqus and Optum GX, while FELA is computed by Optum GX alone. Abaqus will be the main FEA program, and Optum's FEA capabilities will only be used to numerically cross-validate the Abaqus model. Therefore, the Abaqus model is used when referring to FEA, the Optum GX model is used for FELA. Abaqus solves the mechanical problem using traditional finite element methods, while Optum GX solves an optimisation problem of the deformation state corresponding to the applied load using a mixed variational principle.

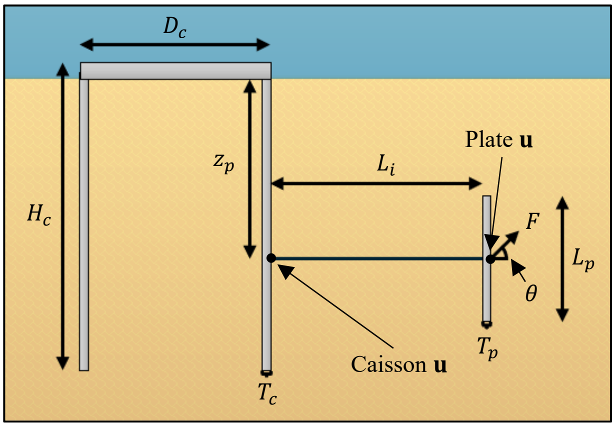

Figure 3. Schematic of CEPAS as it is modelled.

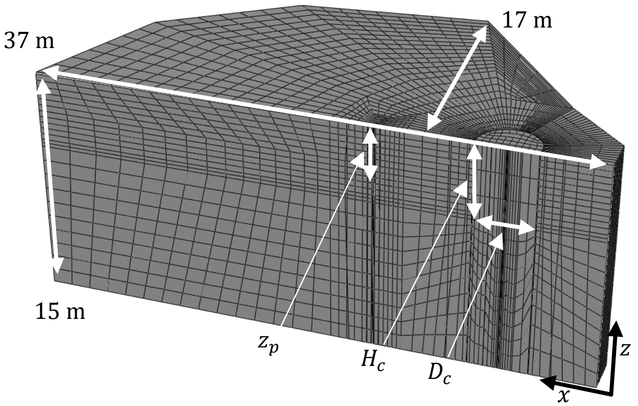

Figure 4. Half of the mesh and main dimensions of the finite element model. The shown mesh is Mesh # 5 in Table 1.

In Abaqus, an in-house UMAT implementation of the MC model (Clausen et al., 2007) is employed for the constitutive behaviour of the soil, including the soil plug within the caisson. This reduces the computational costs and is less prone to convergence issues than the in-built MC model. To secure the numerical stability, a cohesion of $c = 0.5$ kPa is used, while tension cut-off is not assumed. At all soil–steel interfaces, the penalty method is used for a hard pressure-overclosure while assuming a friction coefficient of $\mu = 0.50$ and enabling gap formation. The caisson and plate are modelled using C3D8 elements (three-dimensional eight-node linear brick elements), while the soil is modelled using C3D8R elements (three-dimensional eight-node linear brick elements with reduced integration and hourglass control); the top of the caisson is perfectly tied to the caisson skirt. The intermediate chain is modelled using a wire element, which is a kinematic constraint. It is meshless and ties the chosen degrees of freedom of connector nodes. A link connector section is applied to the wire, which means that the wire constrains the distance between the two points, simulating the action of a rigid intermediate chain under tension; this approach would not be adequate for cyclic loading; however, the analysis of cyclic loading is beyond the scope of the current research. Also, geometrical nonlinearities are enabled in all Abaqus analyses, adopting nonlinear interface behaviour. Finally, as a comparison term, linear analyses are performed by using linear elastic behaviour for all materials, applying surface–surface tie constraints at all interfaces, and disabling geometrical nonlinearities.

In the Optum model, a mixed element type that combines the advantages of upper and lower bound elements is used. Contact is modelled by collapsing patches of regular continuum elements to zero thickness, while the Optum built-in implementation of the MC model is used for the soil. The intermediate mooring line is modelled using a linear connector element (setting a stiffness value so that, at the relevant load ranges, the elongation is negligible, being smaller than 0.1 mm). A remeshing algorithm based on shear dissipation is employed. For each analysis, two mesh adaptivity iterations are performed before the final computation. The adaptivity iterations start at 10 000 elements and aim to use 20 000 elements for the final computation. Otherwise, all model aspects of the Optum model are identical to those of the Abaqus model.

4 MESH SENSITIVITY AND MODEL VALIDATION

As a mesh sensitivity study, to ensure that the Abaqus FEA model is adequately discretised, four mesh configurations with varying refinement were tested for the relatively large-plate system ($L_p = 2.0$ m). These analyses are labelled Mesh # 1–4, spanning from a fine to a coarse mesh, respectively.

Figure 5 shows the total load–displacement curves from horizontal loading, in which "plate displacement" refers to the node of the plate where the load is applied, i.e. the middle front of the plate (see Figure 3). Likewise, later within the text, "caisson displacements" are extracted at the point where the caisson is connected to the intermediate chain (see Figure 3). The applied load gives rise to the in-plane displacement vector $\mathbf{u} = [u_x, u_z]^T$, u_x and u_y being the horizontal and vertical displacements, respectively. Displacements will also be indexed by "caisson" or "plate" depending on which part they refer to.

As key features of the sensitivity study, Table 1 lists the number of degrees of freedom (DOF), the computation time on a computer with Dual Intel Xeon E5-2620 v4 CPUs (2×8 cores running at 2.1 GHz), as well as the relative difference $\Delta_i = (H_{\text{mesh } i,100\text{mm}} - H_{\text{mesh } 1,100\text{mm}})/H_{\text{mesh } 1,100\text{mm}}$ between the horizontal loads leading to total plate displacements of 100 mm with Mesh # i and Mesh # 1, respectively, using Mesh # 1 as the reference case. Lastly, a linear elastic analysis is computed with Mesh # 4, which is reported in Figure 5 to highlight the effect of soil plasticity and nonlinear interface behaviour on the load–displacement curve. Obviously, the effect of these modelling settings is quite significant.

As shown in Figure 5 and quantified by Δ_i in Table 1, the load–displacement curves are nearly mesh independent. The coarser Mesh # 4 shows a deviation of less than 3% compared to the finer Mesh # 1. Further, to compare Optum GX and Abaqus results, Figure 5 plots the load–displacement curve predicted by Optum GX FEA. Interestingly, despite satisfactory agreement up to 50 mm total plate displacement, Optum outcomes exhibit a rapid change in tangent stiffness at approximately 4 MN, beyond which Optum GX results diverge from those of Abaqus. Contrarily, the soil shear deformation mechanisms (omitted) predicted by the two programs are qualitatively similar across the investigated load levels.

Considering the agreement in mobilised horizontal loads and deformation mechanisms, as well as the reduction in computational time of over 80% with respect to the finer mesh,

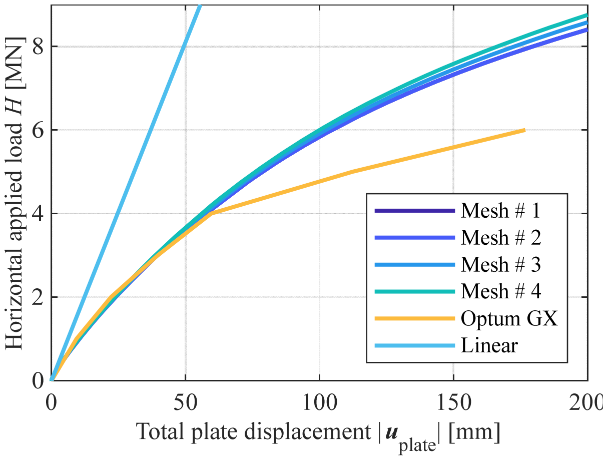

Figure 5. FEA Mesh study of Abaqus model, and its comparison with Optum GX results.

Table 1. DOF and computation time of mesh configurations. Keep in mind that the analyses reached different displacement levels, disturbing somewhat the direct applicability of the computational time metric.

Mesh #	DOF	Computation time [h]	Δ [%]
1	609 066	13.0	0.00
2	382 800	5.5	0.00
3	295 314	6.3	1.34
4	226 629	1.8	2.70

(Mesh # 1), the coarser mesh (Mesh # 4) is selected for all Abaqus FEA in the following sections. Furthermore, the consistency between these two independent numerical tools confirmed the validity of the Abaqus FEA model with Mesh # 4. However, further study is needed to identify the underlying mechanical or numerical reasons for the kink in the load–displacement curve from the Optum GX FEA.

5 RESULTS FOR HORIZONTAL EXTERNAL LOAD

The two CEPAS configurations with different plate sizes are compared to those of their individual components, either the isolated embedded plate, the single caisson, or the single extended-skirt caisson, using FEA and FELA simulations.

5.1 *Limit loads from FELA*

Horizontal capacities from FELA are computed for all configurations with the chosen mixed element type. This means that the horizontal capacities are neither upper nor lower bounds, but rather an approximation to the exact solution. Their mechanical interpretation is supported by the following three capacity ratios:

$$R_{\mathrm{ga}} = \frac{H_{\mathrm{cepas}}}{H_{\mathrm{caisson}}}, \quad R_{\mathrm{vol}} = \frac{H_{\mathrm{cepas}}}{H_{\mathrm{caisson,ext}}}, \tag{1a}$$

$$R_{\mathrm{plate}} = \frac{\left(H_{\mathrm{cepas}} - H_{\mathrm{caisson}}\right)}{H_{\mathrm{plate}}}, \tag{1b}$$

where: (i) R_{ga} is the ratio between the horizontal capacity of CEPAS H_{cepas} and that of the single caisson H_{caisson}, quantifying the plate-induced increase in horizontal capacity; (ii) R_{vol} is the ratio between H_{cepas} and the horizontal capacity $H_{\mathrm{caisson,ext}}$ of a single caisson with an extended skirt so that its volume corresponds to the volume of the original caisson plus the volume of the plate. The load on the extended skirt caisson is applied at the same depth as the intermediate mooring line, z_{p}. R_{vol} provides a measure of the material/cost efficiency of CEPAS; (iii) R_{plate} is the ratio between the plate's horizontal capacity in CEPAS $H_{\mathrm{cepas}} - H_{\mathrm{caisson}}$ and the plate's horizontal capacity when alone, H_{plate}. R_{plate} can also be interpreted as an efficiency ratio, as in $H_{\mathrm{cepas}} = R_{\mathrm{plate}} H_{\mathrm{plate}} + Q_{\mathrm{caisson}}$.

Table 2 summarises the FELA horizontal capacities (and stiffnesses, which will be addressed in the subsequent section) while Table 3 lists the horizontal capacity ratios and stiffness ratios. The relatively small plate ($L_p = 1.0$ m) and large plate ($L_p = 2.0$ m) are addressed as SP and LP, respectively.

First, R_{ga} is discussed. The large-plate CEPAS (LP-CEPAS) has $R_{\mathrm{ga,LP}} = 122\%$, while the small-plate CEPAS (SP-CEPAS) has $R_{\mathrm{ga,SP}} = 116\%$. Thus, the horizontal capacity of the CEPAS is approximately 20% higher than for the single caisson, with a minor increase in horizontal capacity for the LP-CEPAS relative to the SP-CEPAS. However, the SP-CEPAS is much more efficient than the LP-CEPAS in terms of material usage ($R_{\mathrm{vol,LP}} = 64\%$ while $R_{\mathrm{vol,SP}} = 105\%$) which means that SP-CEPAS has a larger horizontal capacity than a caisson with an equivalent material volume. Finally, R_{plate} assesses the efficiency of the plate when integrated into CEPAS. For the LP-CEPAS, $R_{\mathrm{plate,LP}} = 61\%$, while SP-CEPAS has $R_{\mathrm{plate,SP}} = 74\%$. For both the LP-CEPAS and SP-CEPAS, a significant portion of the single plate horizontal capacity is maintained when integrated into the CEPAS, but the SP-CEPAS is clearly the most efficient. In fact, the SP-CEPAS is very efficient in terms of all three ratios, while the LP-CEPAS is less efficient. The next sections investigate horizontal stiffnesses of the two grouped systems and the mechanisms underlying these ratios.

Table 2. FELA horizontal capacities and FEA horizontal stiffnesses. LP abbreviates large plate, SP small plate, ESC extended skirt caisson.

System description	H [kN]	K_{h} [kN/mm]
LP-CEPAS	8 250	162.0
SP-CEPAS	7 795	83.5
Single caisson	6 739	51.7
Single LP	2 493	115.1
Single SP	1 419	27.2
ESC for LP-CEPAS	12 861	70.1
ESC for SP-CEPAS	7 430	54.6

Table 3. Horizontal capacity ratios. LP stands for large plate, SP for small plate.

System description	R_{ga} [%]	R_{vol} [%]	R_{plate} [%]	$R_{\mathrm{ga,Kh}}$ [%]	$R_{\mathrm{vol,Kh}}$ [%]	$R_{\mathrm{plate,Kh}}$ [%]
LP-CEPAS	122	64	61	314	231	96
SP-CEPAS	116	105	74	162	153	117

5.2 *Stiffness from linear elastic FEA*

The stiffness of the CEPASs is studied in this section using linear FEA for both the large- and small-plate CEPASs, since positional restraint at small displacements is of interest in early design. For the sake of simplicity, the horizontal flexibility C_{hh} is inferred as the horizontal displacement u_x of the plate resulting from a unit horizontal force, $H = 1$ N. The study of the vertical flexibility C_{vv} and coupling term C_{hv}, as vertical displacements also occur under horizontal action, is beyond the scope of this paper. For simplicity, if assuming a Winkler spring model of the anchoring at the plate location, the flexibility is converted to a Winkler horizontal stiffness as $K_{\mathrm{h}} = 1/C_{\mathrm{hh}}$. The relationships between horizontal stiffness values for the CEPAS, single plate, single caisson and extended skirt caisson presented in Table 3 are quantified by the same ratios in Eq. (1), defined in terms of horizontal stiffness values, for example, $R_{\mathrm{ga,Kh}} = K_{\mathrm{h,cepas}}/K_{\mathrm{h,caisson}}$.

For LP-CEPAS, $R_{\mathrm{ga,Kh,LP}} = 314\%$, i.e. more than three times the horizontal stiffness of the caisson only, while SP-CEPAS has $R_{\mathrm{ga,Kh,SP}} = 162\%$, i.e. 62% higher than the single caisson. As expected, the plate size influences the CEPAS's overall horizontal stiffness. In terms of stiffness normalized by the extended skirt caisson, for LP-CEPAS $R_{\mathrm{vol,Kh,LP}} = 231\%$, and for CEPAS-SP $R_{\mathrm{vol,Kh,LP}} = 153\%$, meaning that the LP-CEPAS has a horizontal stiffness of more than twice the one of the extended skirt caisson while the SP-CEPAS has a horizontal stiffness about 50% higher than its corresponding extended skirt caisson. Interestingly, this demonstrates a higher stiffness-to-weight ratio of a CEPAS compared with a single caisson, particularly for relatively large plates. Lastly, the LP-CEPAS has an $R_{\mathrm{plate,Kh,LP}} = 96\%$. This means that adding the large plate to the group adds almost the same horizontal stiffness as the large plate had single-handedly; therefore, the linear elastic plate–soil–caisson interaction is minor, with plate–soil and caisson–soil interaction controlling the horizontal stiffness. On the other hand, simulations of the SP-CEPAS and its components gave a stiffness ratio of $R_{\mathrm{plate,Kh,SP}} = 117\%$. This means that adding the small plate to the group contributes more horizontal stiffness than the plate would have single-handedly. This positive interference, i.e. that the plate–soil–caisson interaction increases the overall horizontal stiffness, may be the result of how the Winkler horizontal stiffness is defined here.

5.3 *Load-displacement and deformation results from FEA*

The response to horizontal loading of the two CEPAS configurations is compared both in terms of load-displacement curves as well as load-displacement increment angle curves in Figure 6 and Figure 7, respectively.

First, the load–displacement curves for the CEPAS configurations under horizontal loading are analysed. Figure 6 shows the horizontal (u_x) and vertical (u_z) displacements for both LP-CEPAS and SP-CEPAS. Displacements are reported at the point of external load application on the plate (dashed lines) and at the intermediate chain padeye on the caisson (full line). Positive displacements are defined as upward and in the direction of the applied horizontal load.

The trends in Figure 7 confirm the earlier findings on capacity and stiffness: LP-CEPAS has higher initial stiffness and load capacity than SP-CEPAS. Also, during monotonic loading, the horizontal displacements of the plate and caisson remain similar in the presence of a rigid intermediate chain, which aligns with modelling assumptions. More importantly, this figure highlights some key features of the CEPAS load-displacement response. (i) At low horizontal load levels (up to about 20% of the ultimate horizontal load, or $H < 2$ MN), the horizontal and vertical responses are decoupled. The horizontal displacement increases nearly linearly, while the vertical movement of system remains negligible. This is expected for the caisson, as the chain is attached at a depth close to two-thirds of the skirt length. This tendency is further illustrated by Figure 7. (ii) At intermediate horizontal loads (20%–40% of the ultimate horizontal load, or 2 MN $< H < 4$ MN), the system's response becomes coupled. The plate first begins to move vertically, followed by the caisson, although the vertical movements remain smaller than the horizontal ones. This decoupling is obvious in Figure 7. (iii) At higher load levels (>40% of the ultimate horizontal load, or $H > 4$ MN), both the plate and the caisson experience vertical displacements at a progressively increasing rate, while the horizontal displacement rate is nearly constant. The incremental displacement vector ($\Delta\mathbf{u} = [\Delta u_x, \Delta u_z]$) becomes inclined at an angle $\alpha = 15°$–$30°$ to the horizontal for the caisson, and $\alpha = 30°$–$45°$ for the plate, cf. Figure 7. Across (ii) and (iii), the vertical displacements of the plate are higher than those of the caisson, and the differential grows with load, leading to an increasingly inclined force being transmitted from the plate to the caisson.

A key difference between the SP- and LP-CEPAS is observed: (a) The caisson's $H{-}u_x$ and $H{-}u_z$ curves scale with the overall system stiffness. Since upward movement of the caisson requires horizontal displacement, and horizontal displacement is larger in the SP-CEPAS, the small-plate system results in greater caisson uplift; (b) Despite their size difference, the plates in both systems show similar vertical displacements across load levels. This is likely due to the roto-translational behaviour of the plate, as later discussed. To relate the observed load-displacement curves to the ground deformation pattern, Figure 8 presents the total displacement magnitude along a vertical cross-section through the centre of the LP-CEPAS, under high horizontal loading ($H = 8$ MN). In this figure, when the plate and caisson respond with coupled translational motion in both the x and z directions, the soil in front of the loaded plate exhibits a displacement pattern resembling a passive wedge: the deformation extends from the plate tip to the soil surface, with contour lines inclined close to the horizontal, indicating a wedge moving both horizontally and vertically, consistent with the behaviour seen in Figure 6.

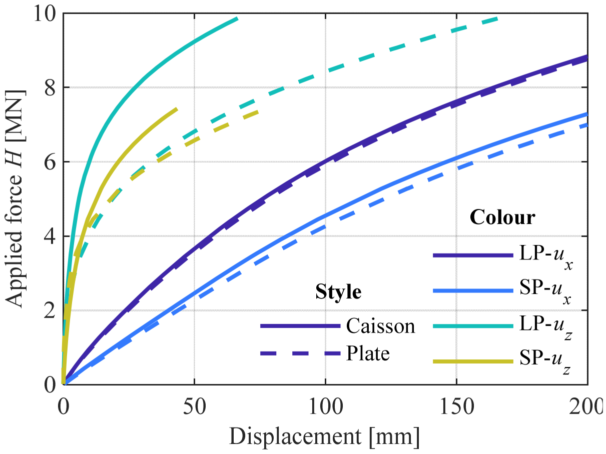

Figure 6. Displacements of plate and caisson for LP-CEPAS and SP-CEPAS because of horizontal load.

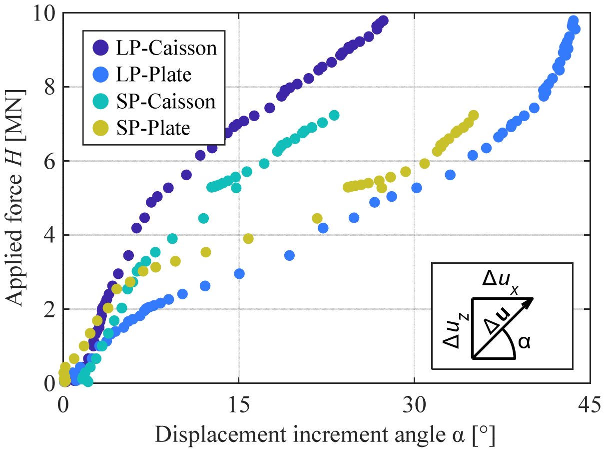

Figure 7. Displacement increment angles to the horizontal for CEPAS at the caisson and plate control nodes because of horizontal load.

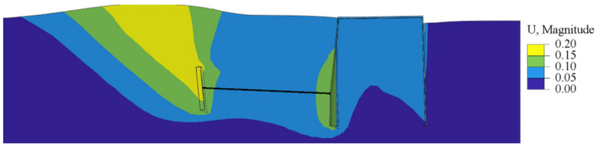

Figure 8. Total displacement contours of the subsurface soil for the LP-CEPAS at the horizontal load $H = 8$ MN. The displacements have been scaled by a factor of 5.

More importantly, a distinct soil block, encompassing the soil inside the caisson and the soil between the caisson skirt and the plate, displaces nearly as a rigid body, except for localised deformation near the loaded portion of the skirt. A prominent, nearly horizontal shear band (results omitted) forms between the caisson toe and the plate tip, contributing significantly to the system's load capacity. This block mechanism underpins the efficiency of the CEPAS in terms of stiffness-to-weight and strength-to-weight ratios, as discussed in Section 5.

The corresponding results for the SP-CEPAS (omitted) suggest that both the frontal wedge and block mechanism exhibit more complex geometries. However, these differences do not significantly affect the overall load–displacement behaviour when comparing the SP- and LP-CEPAS, as seen in Figure 6, which are qualitatively similar. The next section examines how the inclination of the external load affects the CEPAS response at the plate loading point.

6 PERFORMANCE-BASED INTERACTION DIAGRAM FOR INCLINED LOADING

As a preliminary study, an interaction diagram is developed for the LP-CEPAS to describe its response under inclined loading. The diagram is based on post-processing the results from 10

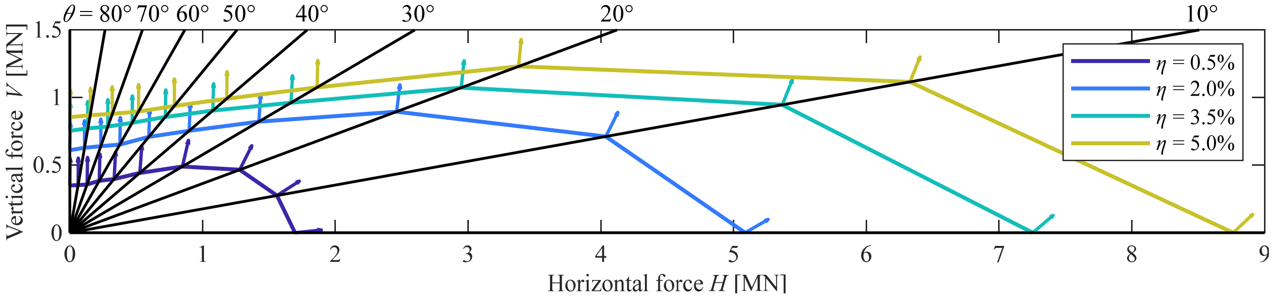

Figure 9. Performance-based interaction diagram of the LP-CEPAS. The arrows on each line indicate the direction of the displacement increment at this capacity and with the given load inclination.

FEA simulations with load inclinations ranging from $\theta = 0°$ (purely horizontal) to $\theta = 90°$ (purely vertical).

Figure 9 shows the interaction diagram in the (H, V) load space, where H and V are the horizontal and vertical components of the applied load vector $\mathbf{F}$. Each isoline represents combinations of H and V that produce the same plate displacement level η, defined as the displacement parallel to the load direction ($u_{\parallel \boldsymbol{F},\mathrm{plate}}$) normalised by the caisson diameter ($\eta = u_{\parallel \boldsymbol{F},\mathrm{plate}}/D_\mathrm{c}$). Arrows of unit length are plotted along these isolines to indicate the direction (versor) $\Delta\hat{\mathbf{u}}_\mathrm{plate}$ of the incremental displacement vector $\Delta\mathbf{u}_\mathrm{plate} = [\Delta u_x, \Delta u_z]^T$ at that deformation state.

Across all displacement levels η, the maximum mobilised load occurs under horizontal loading ($\theta = 0°$), consistent with the earlier discussion of Figure 6. As the load and η increase, the direction of the incremental displacement versor $\Delta\hat{\mathbf{u}}$ progressively rotates towards the vertical direction, even for purely horizontal loading. Interestingly, the maximum vertical capacity for a given η is not reached at $\theta = 90°$, but rather at $\theta \approx 20°$, due to the concave shape of the interaction isolines. This shape likely arises from the coupling between vertical and horizontal displacements – especially at load inclinations θ above 30°, where the incremental displacement direction $\Delta\hat{\mathbf{u}}_\mathrm{plate}$ becomes nearly vertical.

This interaction diagram can serve as a basis for estimating reduction factors in horizontal capacity when the system is subjected to inclined loading. Such reductions are particularly relevant for catenary and semi-taut mooring systems, given the embedded configuration of the external mooring line and the resulting inclination of the load it transmits to the anchor.

7 CONCLUSIONS

This study introduced and evaluated the caisson–embedded-plate-anchor system (CEPAS) as a novel grouped anchoring concept for floating offshore wind turbines. Several practical advantages of the CEPAS over conventional single caisson designs were identified.

Finite element analyses indicated that CEPAS can outperform a single caisson of equivalent steel volume under monotonic loading, particularly in terms of strength-to-weight ratio, while the linear elastic horizontal stiffness is nearly equal to the superposition of individual plate and caisson components. For the cases considered, the overall load–displacement mechanisms were not strongly dependent on plate size relative to the caisson. Both the LP-CEPAS and SP-CEPAS configurations exhibited similar responses under horizontal loading: pure horizontal translation at low loads and coupled vertical–horizontal movement at higher loads. However, the small-plate CEPAS demonstrated more efficient and integrated behaviour, suggesting that relatively small plates may be sufficient to achieve optimal performance while positioning the mooring line at the desired depth. A preliminary analysis quantified the response of the LP-CEPAS under inclined loading at the plate by developing a performance-based interaction diagram, which links displacement levels to load capacities at various inclinations.

Future research will address several areas beyond the scope of this study. These include a detailed evaluation of the CEPAS under inclined loading conditions, the influence of alternative intermediate chain layouts, the impact of installation effects, and improved understanding of the plate–soil–caisson interaction through a condensed flexibility matrix approach. Lastly, physical model tests will be performed in subsequent papers to validate numerical findings. Furthermore, field-scale validation is recommended.

ACKNOWLEDGEMENTS

This research has been funded by Independent Research Fund Denmark via the project “A novel grouped anchor concept for floating offshore wind turbines” (grant no. 4286-00115B).

REFERENCES

Barter, G., Robertson, A., & Musial, W. (2020). A systems engineering vision for floating offshore wind cost optimization. *Renewable Energy Focus*, 1-16.

Cerfontaine, B., White, D., Kwa, K., Gourvenec, S., Knappett, J., & Brown, M. (2023). Anchor geotechnics for floating offshore wind: Current technologies and future innovations. *Ocean Engineering*, 114327.

Clausen, J., Damkilde, L., & Andersen, L. (2005). Efficient return algorithms for associated plasticity with multiple yield planes. *International Journal for Numerical Methods in Engineering, 66*(6), 1036-1059.

Dührkop, J., Grabe, J., Bienen, B., White, D., & Randolph, M. (2010). Centrifuge experiments on laterally loaded piles with wings. *Proceedings of the 7th International Conference on Physical Modeling in Geotechnics*, (pp. 919-924).

International Energy Agency. (2019). *Offshore Wind Outlook 2019.*

Ong, S., Campbell, C., Denholm, P., Margolis, R., & Heath, G. (2013). *Land-Use Requirements for Solar Power Plants in the United States.*

Rui, S., Wang, L., Zhou, Z., Jostad, H. P., & Guo, Z. (2024). Bearing performance of a novel caisson-plate gravity anchor. *Géotechnique, 75*(5), 686-697.

Stehly, T., Beiter, P., & Duffy, P. (2020). *2019 Cost of Wind Energy Review.*

Walker, G. R., & Taylor, R. J. (1984, November). Model Anchors Tests in Cohensionless Soil. *Journal of Waterway, Port, Coastal and Ocean Engineering, 110*(4), 463-471.